Journal of Physics: Conference Series **2374** (2022) 012059 doi:10.1088/1742-6596/2374/1/012059

Performance and running experience of the Belle II silicon vertex detector

K. R. Nakamura[18,15], K. Adamczyk[20], L. Aggarwal[9], H. Aihara[17], T. Aziz[10], S. Bacher[20], S. Bahinipati[6], G. Batignani[11,12], J. Baudot[5], P. K. Behera[7], S. Bettarini[11,12], T. Bilka[3], A. Bozek[20], F. Buchsteiner[2], G. Casarosa[11,12], L. Corona[11,12], T. Czank[16], S. B. Das[8], G. Dujany[5], F. Forti[11,12], M. Friedl[2], A. Gabrielli[13,14], E. Ganiev[13,14], B. Gobbo[14], S. Halder[10], K. Hara[18,15], S. Hazra[10], T. Higuchi[16], C. Irmler[2], A. Ishikawa[18,15], H. B. Jeon[19], Y. Jin[13,14], C. Joo[16], M. Kaleta[20], A. B. Kaliyar[10], J. Kandra[3], K. H. Kang[19], P. Kapusta[20], P. Kodyš[3], T. Kohriki[18], M. Kumar[8], R. Kumar[9], C. La Licata[16], K. Lalwani[8], S. C. Lee[19], J. Libby[7], L. Massaccesi[11,12], S. N. Mayekar[10], G. B. Mohanty[10], T. Morii[16], Z. Natkaniec[20], Y. Onuki[17], W. Ostrowicz[20], A. Paladino[11,12], E. Paoloni[11,12], H. Park[19], G. Polat[4], K. K. Rao[10], I. Ripp-Baudot[5], G. Rizzo[11,12], D. Sahoo[10], C. Schwanda[2], J. Serrano[4], J. Suzuki[18], S. Tanaka[18,15], H. Tanigawa[17], R. Thalmeier[2], R. Tiwari[10], T. Tsuboyama[18,15], Y. Uematsu[17], O. Verbycka[20], L. Vitale[13,14], K. Wan[17], Z. Wang[17], J. Webb[1], J. Wiechczynski[12], H. Yin[2], L. Zani[4]

(Belle II SVD Collaboration)

[1]School of Physics, University of Melbourne, Melbourne, Victoria 3010, Australia
[2]Institute of High Energy Physics, Austrian Academy of Sciences, 1050 Vienna, Austria
[3]Faculty of Mathematics and Physics, Charles University, 121 16 Prague, Czech Republic
[4]Aix Marseille Université , CNRS/IN2P3, CPPM, 13288 Marseille, France
[5]IPHC, UMR 7178, Université de Strasbourg, CNRS, 67037 Strasbourg, France
[6]Indian Institute of Technology Bhubaneswar, Satya Nagar, India
[7]Indian Institute of Technology Madras, Chennai 600036, India
[8]Malaviya National Institute of Technology Jaipur, Jaipur 302017, India
[9]Punjab Agricultural University, Ludhiana 141004, India
[10]Tata Institute of Fundamental Research, Mumbai 400005, India
[11]Dipartimento di Fisica, Università di Pisa, I-56127 Pisa, Italy
[12]INFN Sezione di Pisa, I-56127 Pisa, Italy
[13]Dipartimento di Fisica, Università di Trieste, I-34127 Trieste, Italy
[14]INFN Sezione di Trieste, I-34127 Trieste, Italy
[15]The Graduate University for Advanced Studies (SOKENDAI), Hayama 240-0193, Japan
[16]Kavli Institute for the Physics and Mathematics of the Universe (WPI), University of Tokyo, Kashiwa 277-8583, Japan
[17]Department of Physics, University of Tokyo, Tokyo 113-0033, Japan
[18]High Energy Accelerator Research Organization (KEK), Tsukuba 305-0801, Japan
[19]Department of Physics, Kyungpook National University, Daegu 41566, Korea
[20]H. Niewodniczanski Institute of Nuclear Physics, Krakow 31-342, Poland

E-mail: katsuro.nakamura@kek.jp

Abstract. The Belle II silicon vertex detector is one of the vertex detectors in the Belle II experiment. The detector reads out the signals from the double-sided silicon strip sensors with the APV25 front-end readout ASIC, adopting the chip-on-sensor concept to minimize the strip noise. The detector has been operated in the experiment since the spring of 2019. Analyzing the acquired data during the beam collisions, the excellent performance of the detector is confirmed. Also, the radiation dose and 1-MeV equivalent neutron fluence of the detector are estimated using the measured dose rates of the diamond sensors installed on the beam pipe and are compared with the measured radiation effects in the strip noise, leakage current, and depletion voltage. This paper briefly introduces the main features of the silicon vertex detector, and then reports on the measured performance and radiation effects of the first two years of running experience of the detector.

1. Introduction

The Belle II experiment [1] is a luminosity-frontier experiment exploring new physics beyond the standard model with the SuperKEKB accelerator [2] which provides 7 GeV electron and 4 GeV positron collisions at the center of mass energy of 10.58 GeV. The target peak luminosity and integrated luminosity of the Belle II experiment are 6×10^{35} cm^{-2}s^{-1} and 50 ab^{-1}, respectively. The experiment with the full detector system has been operated since March 2019.

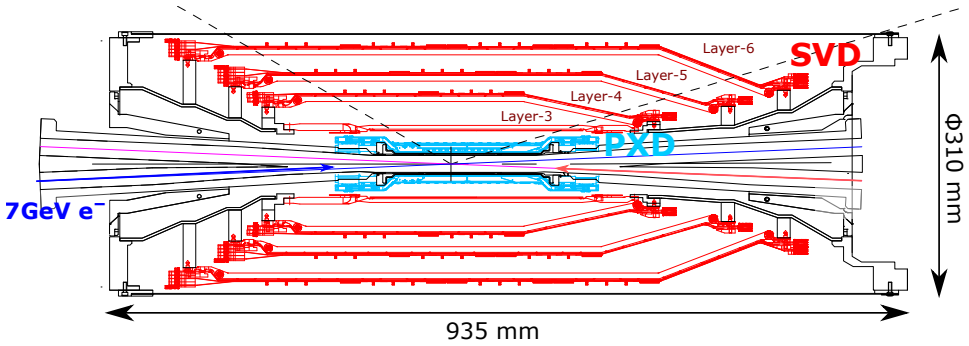

Figure 1. The cross-section view of the vertex detectors. The SVD is represented with red color, while PXD is with light blue color. The locations of the diamond sensors installed on the beam pipe are indicated with green circles.

Figure 1 shows the cross-section view of the vertex detectors in Belle II. The vertex detectors consist of the two-layers pixel detector (PXD) made of DEPFET sensors, and the four-layers silicon vertex detector (SVD), which is made of ladders with double-sided silicon strip detectors (DSSD). The SVD plays the roles of the extrapolation of the reconstructed particle trajectories to PXD, standalone tracking, and particle identification using the SVD's dE/dx information.

2. Belle II silicon vertex detector

The SVD consists of four layers of ladders, named layer-3, layer-4, layer-5, and layer-6, from inner to outer. The number of ladders per layer is 7 in the layer-3, 10 in the layer-4, 12 in the layer-5, and 16 in the layer-6. In the layer-4, 5, 6, the ladder has a slanted part. The averaged material budget per layer is 0.7% X_0. Also, diamond sensors [3] are installed on the beam pipe near the interaction point, as shown with green circles in figure 1. These diamond sensors are used both in the beam abort system and to measure the radiation dose rates on the beam pipe, which are used to evaluate the dose rate on the SVD as described in section 5.

The DSSD sensor for the SVD is fabricated based on the n-substrate wafer. The readout strips have the AC-coupling that is made of the SiO_2 capacitance layer between the implant

	Small rectangle	Large rectangle	Trapezoid
Readout strips p-side	768	768	768
Readout strips n-side	768	512	512
Readout pitch p-side	50 µm	75 µm	$50 - 75$ µm
Readout pitch n-side	160 µm	240 µm	240 µm
Sensor thickness	320 µm	320 µm	300 µm
Manufacturer	HPK	HPK	Micron

Table 1. Geometrical specifications of the double-sided silicon strip sensors used in the SVD. The sensors have three types, namely small and large rectangles, and trapezoid. All sensors have one intermediate floating strip between two readout strips.

and aluminum layers. There is a floating strip between two adjacent readout strips in both the p- and n-sides. The sensors have three types of design, small rectangle, large rectangle, and trapezoid.

The number of readout strips, readout pitches, thickness, and manufacture are summarized in table 1. The small and large rectangular sensors are produced in HPK, while the trapezoidal sensors are produced in Micron. All sensors in the layer-3 are small sensors that have the finest readout pitches, 50 µm in the p-side and 160 µm in the n-side. In all sensors, the n-side strips have larger pitches than the p-side strips. The sensor thickness is 320 µm for HPK sensors and 300 µm for Micron sensors. The full depletion voltage is about 40-60 V for the HPK sensors, while it is about 20-40 V for the Micron sensors. The operation bias voltage of the sensors is 100 V. In total, the SVD has 172 DSSD sensors and 224k readout strips.

The front-end readout ASIC in the SVD is the APV25 chip [4], which was developed for the CMS silicon tracker. The APV25 chip has a short shaping time of 50 ns and a high radiation tolerance of more than 100 Mrad. The number of the input channels per chip is 128. In the current data acquisition mode, the six subsequent analog samples are read out with a 32 MHz clock to reconstruct the signal waveform. The power consumption of the APV25 chip is 0.4 W per chip in maximum. Because the SVD has 1748 chips, the maximum heat dissipation from the SVD ladders is about 700 W in total.

The novel idea used in the ladder design is the chip-on-sensor concept. In this concept, the chips are located on the sensor with a thermal isolation foam in between. This design minimizes the strip noise because it minimizes the signal propagation length that is a source of the capacitive noise on the channel. More details on the ladder design and construction can be found in a reference [5].

3. SVD operational experience in the Belle II experiment

The SVD was installed in the Belle II detector in November 2018 and has operated in the physics data taking since March 2019. The SuperKEKB accelerator is improving the performance year after year, and the peak delivered luminosity reaches 3.12×10^{34} cm^{-2}s^{-1} in June 2021. The SVD operation has been reliable and smooth. The SVD has only a few defective strips, and the total fraction of the masked strips among all strips is less than 1%. They are mainly due to the initial defects caused in the sensor production. A few additional defects were created in the ladder assembly or developed during the operation.

There were a few troubles in the SVD operation so far. At the beginning of the SVD operation in the spring of 2019, the output signal from one APV25 chip in the layer-3 sensor out of 1748 chips became distorted and could not be properly decoded in the readout electronics. Then, this APV25 chip was disabled and masked in the readout. This issue was investigated in the summer of 2019, and we concluded it was due to a loose cable connection as the cable reconnection cured

the problem. After this incident, all the APV25 chips are working stably for more than two years. Another minor incident was that 10 new pinholes, which are the broken SiO_2 capacitors on the sensor strips, were created at a huge beam loss incident that happened in June 2019. For large bursts of radiation, the charge released inside the silicon could cause a large fraction of the bias voltage to drop on these integrated decoupling capacitors. Although the capacitor breakdown voltage is in general well above 100V, and all strips have been tested up to 20V, a few weaker capacitors, with lower voltage rating, could be damaged by the huge beam loss incident. While such huge beam losses happened several times after the incident, no additional pinhole has been observed so far.

4. SVD performance

The data taken during the beam collisions are analyzed and the excellent performance of the SVD is confirmed. In this section, the results of the cluster charge and signal-to-noise ratio distributions, the hit efficiency, the position resolution, and the hit time resolution are described.

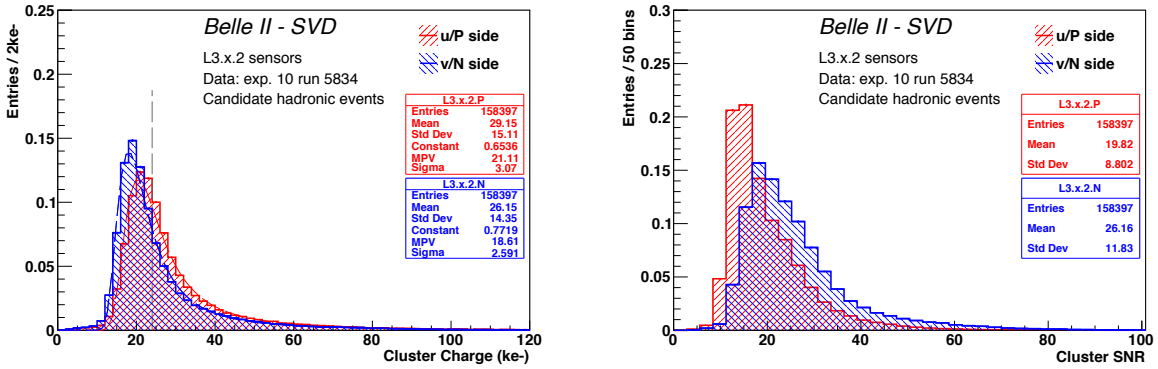

(a) Normalized cluster charge

(b) Cluster signal-to-noise ratio

Figure 2. Distributions of (a) cluster charge normalized with the track path length and scaled to the sensor thickness 320 µm and (b) cluster signal-to-noise ratio of sensors in the layer-3. The red and blue distributions correspond to the p-side and n-side, respectively. The dashed line in the cluster charge distribution represents an expected MPV of the MIP signal, 24 ke^-.

The cluster charge distributions are studied by analyzing data taken in December 2019. The distribution depends on the incident angle of the particle on the sensor, because the traverse path in the sensor, and then the energy deposition, scales as $d/\cos\theta$, where d is the sensor thickness and θ is the incident angle. Figure 2(a) shows the cluster charge distributions of both the p-side and n-side in layer-3 sensors, in which the cluster charges are normalized with the path length and scaled to the sensor thickness. The figure also shows the expected most probable value (MPV) for the MIP signals in the 320 µm thickness sensor, 24 ke^-. The fit with the Landau distribution to the p-side distribution results in a MPV of 21 ke^-. Those two values are fairly consistent, taking into account the large uncertainty of about 15% in the absolute gain calibration [6], which is used to convert the cluster charge in the unit of the number of electrons. On the other hand, the n-side distribution shows about 12% smaller MPV than the p-side. It is expected because the n-side has the floating strips with the wider strip pitch than the p-side, and therefore a larger capacitive coupling to the back side, which causes the signal loss.

The signal-to-noise ratio (SNR) for clusters indicates the significance of the cluster signals to distinguish them from the electrical noise fluctuation. The cluster SNR is defined as the total charge in the cluster divided by the square root of the quadratic sum of the noises on the strips

associated with the cluster. The cluster SNR distributions in both the p-side and n-side are shown in figure 2(b). In contrast to the larger signal charge in the p-side than in the n-side as seen above, the strip noise in the p-side, 740-960 e^-, is larger than in the n-side, 510-680 e^-, because of the longer strip length and the smaller strip pitch. Therefore, in total, the MPV of the SNR distribution in the p-side is smaller than in the n-side. The resulting MPVs of the SNR distributions in all sensors range from 13 to 30. The values depend on the sensor side and location, which corresponds to different incident angles.

Excellent hit efficiencies in all sensors with good stability during the operation are confirmed. The efficiency averaged over sensors is above 99.5%. A few sensors have about 98% due to more defect strips than others, which were already observed during the module assembly.

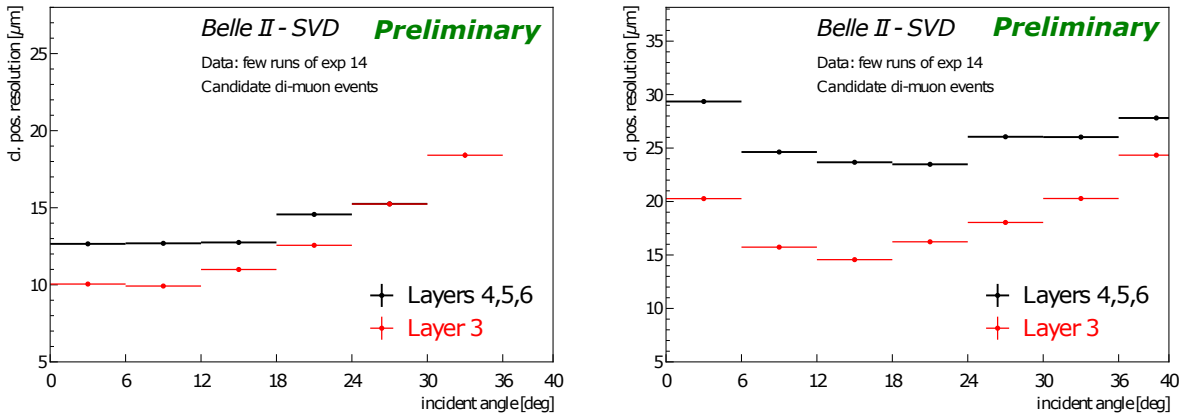

(a) p-side (b) n-side

Figure 3. The hit position resolutions (a) in the p-side and (b) in the n-side, as a function of the projected incident angle.

The hit position resolution depends on the incident angle of the particle trajectory projected to the plane perpendicular to the strip direction. Figure 3 shows the measured position resolutions as a function of the projected incident angle. The measured resolution in the layer-3 ladders, which have the finest strip pitches, is 10-20 µm in the p-side and 15-25 µm in the n-side for the projected incident angle of less than 40 degrees. While the excellent resolution is confirmed, the measurement method is being optimized furthermore for better accuracy of the estimated resolutions.

The hit time for clusters is calculated using the hit information of the six subsequent samples. The hit time resolutions are measured by comparing the calculated hit time with the event time evaluated by other detectors that have good time resolution, about 0.7 ns. The measured hit time resolutions of the SVD are 2.9 ns for the p-side and 2.4 ns for the n-side. The hit time resolution is important to reject off-time hits of the beam background, and the rejection of the background hit with the hit time selection is being integrated.

5. Radiation effect on SVD

The beam background causes the radiation damage and the increase of the hit rate and occupancy that can degrade the SVD performance. Therefore, the study of the beam background amount on the SVD is important to estimate how these effects evolve in the future accelerator condition. For the SVD, the hit occupancy is used as an index of the beam background rate.

Larger background occupancy increases the number of the cluster candidates that can be erroneously associated to track or create fake tracks in the reconstruction and degrades the

tracking performance. Also, larger beam background rate increases the radiation damages of sensors. At present, the degradation of the tracking performance gives the tightest upper limit of the hit occupancy, and this corresponds to about 2-3% occupancy in the layer-3. With the new background rejection based on the hit time selection this limit can be relaxed by a factor of about 2, while the more precise estimation of the new limit is being investigated.

During the operation in the spring of 2021, the averaged hit occupancy in the layer-3 sensors was less than 0.5%, which is well below the present limit. Projection of the hit occupancy at the original designed luminosity (8×10^{35} cm^{-2}s^{-1}) is estimated by the Monte-Carlo (MC) simulation result corrected by the scaling ratio between data and MC, measured in dedicated beam background studies. The projected hit occupancy is 4.1% for the layer-3, 2.1% for the layer-4, 1.7% for the layer-5, and 1.1% for the layer-6. While the layer-3 occupancy exceeds the present limit, it is expected to be acceptable once the new background rejection is integrated. The projection also estimates the dose rate and equivalent neutron fluence to be about 300 krad per Snowmass year and about 4.5×10^{11} $n_{\rm eq}$/cm^{-2} per Snowmass year, respectively, where a Snowmass year is defined as 10^7 s.

The integrated dose in the DSSD sensors is evaluated exploiting the good correlation between the measured SVD occupancy and the dose rate measured in the diamond sensors with the following method. The correlation coefficient between the diamond sensors, always ON, and the SVD hit occupancy in each layer are measured on data. The conversion factor from the hit occupancy to the dose rate in the sensor is evaluated by the MC simulation. Using this method, a preliminary estimate of the integrated dose in the DSSD sensors was performed using the measured diamond integrated dose until the end of 2020, corresponding to the first two years of operation. This estimate is still affected by a large uncertainty and a more accurate analysis is now under development. The spatial beam background distribution shows a maximum in the middle plane, which is defined as the horizontal plane formed by the crossing electron and position beamlines. The integrated dose in the layer-3 middle-plane sensors is 140 krad, and the average of the integrated dose in each layer is about 100 krad for the layer-3, 20-30 krad for the layer-4, 5, and 6. Also, by applying another conversion factor from the radiation dose to the 1-MeV equivalent neutron fluence that was evaluated by the MC simulation, 1.5×10^{12} $n_{\rm eq}$/cm^2/Mrad, the integrated amount of 1-MeV equivalent neutron in the layer-3 middle-plane sensors over the two-years operation is estimated to be 2.1×10^{11} $n_{\rm eq}$/cm^2.

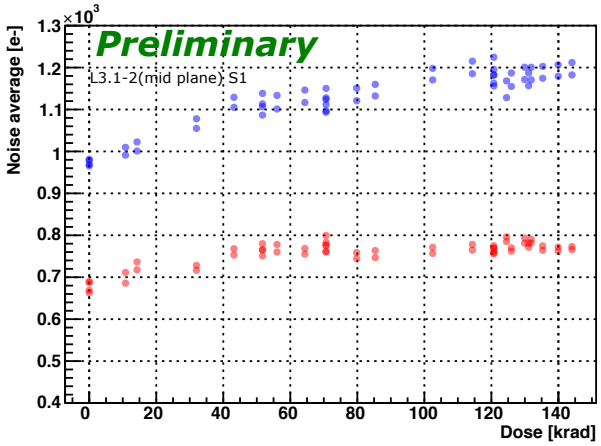

Figure 4. Averaged noise in the layer-3 middle-plane sensors as functions of the integrated dose. Blue and red points are the results in the p-side and n-side, respectively.

As a radiation effect, the ionizing energy loss in the sensor surface creates the fixed charge in the oxide layer, which increases the inter-strip capacitance and therefore the strip noise. The

averaged noise in the layer-3 middle-plane sensors as a function of the integrated dose is shown in figure 4. The noise in the p-side is increased by up to 25% after the irradiation of about 140 krad, and even smaller on the n-side. In both cases, the increase is not affecting the performance. The increase in the fixed oxide charge is expected to be saturated at some point. The saturation is already seen in the n-side and starting to be seen in the p-side.

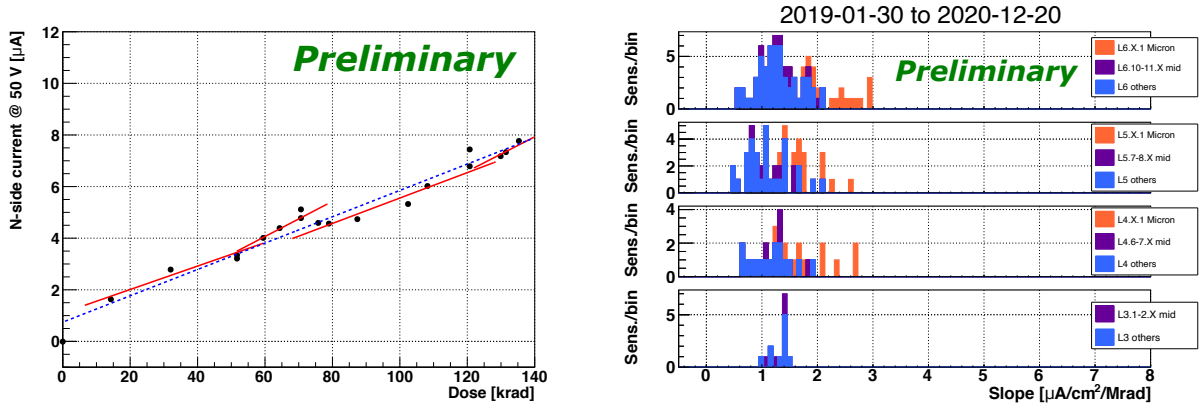

(a) Leakage current vs. integrated dose

(b) Slope distributions

Figure 5. (a) Leakage current in the layer-3 middle-plane sensor as a function of the integrated dose. The red lines are the linear fitting results for each Belle II operation period, and the blue dot line is the linear fitting result over two-year operation. (b) Distributions of slopes of the linear fitting results for all sensors in the layer-6, 5, 4, and 3 from top to bottom.

The increase in the sensor leakage current is also a radiation effect, that is caused by the sensor bulk damage due to the non-ionizing energy loss and by surface generation current due to defects at the Si/SiO2 interface induced by ionizing damage. Figure 5(a) shows the leakage currents in the layer-3 middle-plane sensor as a function of the integrated dose over the two-year operation. An excellent linear correlation between them is seen. Fitting with a linear function, the leakage current increase rate is measured by the slope of the line. Figure 5(b) shows the distributions of the leakage current increase rates in all sensors. Consistent coefficients of about 1-2 μA/cm^2/Mrad are obtained. They are the same order of the previous BaBar measurement, about 1 μA/cm^2/Mrad at 20 °C [7]. The widths of the distributions are due to temperature effects and the dose spread among sensors in the layer while an averaged dose in each layer is used for all sensors in the measurement. From the result, after 10 Mrad irradiation, the increase of the leakage current per strip in the layer-3 middle-plane sensor will be about 0.5 μA/strip. This increase does not affect the strip noise significantly because of the short shaping time (50 ns) of the APV25 chip.

The sensor bulk damage also changes the depletion voltage. Since the substrate of the SVD DSSD sensors is n-type, the bias voltage develops the sensor depletion from the p-side strips toward the n-side strips. Accordingly, the n-side strips are insulated when the full depletion is reached and the noise drops to a minimum level. Using this feature, the full depletion voltage has been monitored time-to-time since July 2020 by measuring the n-side strip noise as a function of the bias voltage. Figure 6 shows the averaged strips noise in the layer-3 middle-plane sensor as a function of the bias voltage, which was measured on different dates. The noise reaches a minimum level at the bias voltage of about 60 V, which corresponds to the full depletion voltage of the sensor. From the diamond dose measurement, the integrated equivalent neutron fluences in the sensor on those dates are estimated to be about 1.8, 1.95, and 2.1×10^{11} $n_{\rm eq}$/cm^2. No

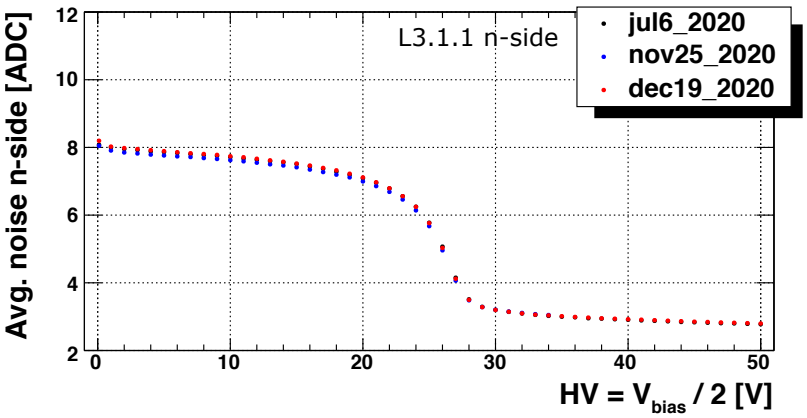

Figure 6. The averaged n-side strip noise in the layer-3 middle-plane sensor as functions of applied bias voltage on the sensor. Results of three measurements on different dates (6th Jul. 2020, 25th Nov. 2020, and 19th Dec. 2020) are shown.

visible change in the functional shape is observed among the three results. Since the integrated equivalent neutron fluence is still very small, the observation is consistent with our expectation.

6. Conclusion and prospect

The Belle II silicon vertex detector has been operated since 2019 and is running smoothly and reliably with excellent performance. The integrated dose and the integrated equivalent neutron fluence in the layer-3 middle-plane sensor until the end of 2020, corresponding to the first two years of operation, are estimated to be 140 krad and 2.1×10^{11} $n_{\rm eq}/{\rm cm}^2$, respectively. In the spring of 2021, the hit occupancy in the layer-3 is below 0.5%, and effects of the radiation damage started to be seen in the strip noise and sensor leakage current. They are consistent with the expectation and do not affect the SVD performance.

Several improvements of the SVD in the future are planned and the development is ongoing. The hit time selection will be integrated to reject the off-time beam background hits. This will relax the limit of the hit occupancy to accept the projected hit occupancy. The optimization of the position resolution measurement is being studied for better accuracy. Also, a new data-acquisition mode in the APV25 chip will be integrated to reduce the number of readout analog samples per trigger and therefore the data size.

Acknowledgment

This project has received funding from the European Union's Horizon 2020 research and innovation programme under the Marie Sklodowska-Curie grant agreements No 644294 and 822070. This work is supported by MEXT, WPI, and JSPS (Japan); ARC (Australia); BMWFW (Austria); MSMT (Czechia); CNRS/IN2P3 (France); AIDA-2020 (Germany); DAE and DST (India); INFN (Italy); NRF and RSRI (Korea); and MNiSW (Poland).

References

[1] T. Abe et al., Belle II Technical Design Report (2010), arXiv:1011.0352.
[2] Y. Ohnishi et al., Accelerator Design of SuperKEKB, Prog. Theor. Exp.Phys **2013**, 03A011 (2013).
[3] S. Bacher et al., Nucl. Instrum. Meth. A **997** (2021) 165157.
[4] M.J. French et al., Nucl. Instrum. Meth. A **466** (2001) 2.
[5] K. Adamczyk et al., Nucl. Instrum. Meth. A, **845** (2017) 38.
[6] M. Raymond et al., 11th Workshop on Electronics for LHC and Future Experiments (LECC 2005) 91 (2005).
[7] B. Aubert et al., Nucl. Instrum. Meth. A **729** (2013) 615.